Analytica Chimica Acta 1156 (2021) 338329

Contents lists available at ScienceDirect

Analytica Chimica Acta

journal homepage: www.elsevier.com/locate/aca

Development of an open-source thermally stabilized quartz crystal microbalance instrument for biomolecule-substrate binding assays on gold and graphene

Daniel Meléndrez [a], Piramon Hampitak [a], Thomas Jowitt [b], Maria Iliut [a], Aravind Vijayaraghavan [a, *]

[a] Department of Materials and National Graphene Institute, The University of Manchester, Oxford Road, Manchester, M13 9PL, UK
[b] School of Biological Sciences, Faculty of Biology Medicine and Health, The University of Manchester, Oxford Road, Manchester, M13 9PL, UK

HIGHLIGHTS

- The cQCM is an open-source point-of-care biosensor instrument.
- Close-loop thermal stabilization is implemented to deliver reproducible performance.
- The low-cost and field-serviceable instrument is ideally suited for low- and middle-income countries.
- The graphene-coated G-QCM chip offers a novel binding interface.
- The instrument could be used for disease screening and rapid therapeutics development.

GRAPHICAL ABSTRACT

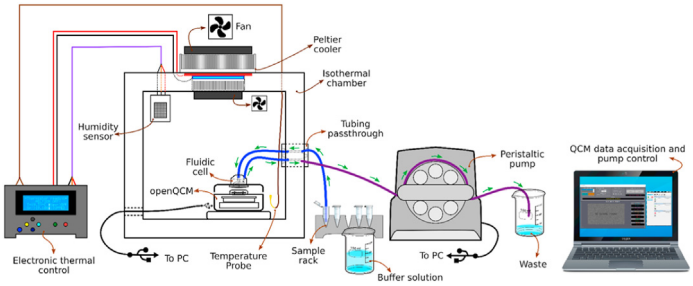

ARTICLE INFO

Article history:
Received 2 October 2020
Received in revised form
20 January 2021
Accepted 14 February 2021
Available online 8 March 2021

Keywords:
Quartz crystal microbalance
Bovine serum albumin
Reduced graphene oxide
Biosensor
Open-source

ABSTRACT

The interaction of biomolecules, such as proteins, with biomaterial surfaces is key to disease diagnostic and therapeutic development applications. There is a significant need for rapid, low-cost, field-serviceable instruments to monitor such interactions, where open-source tools can help to improve the accessibility to disease screening instruments especially in low- and middle-income countries. We have developed and evaluated a low-cost integrated quartz crystal microbalance (QCM) instrument for biomolecular analysis based on an open-source QCM device. The custom QCM instrument was equipped with a custom-made electronically controlled isothermal chamber with a closed-loop control routine. A thermal coefficient of 5.6 ppm/°C was obtained from a series of evaluations of the implemented control. Additionally, a custom-designed data acquisition system and a mathematical processing and analysis tool is implemented. The quartz crystal detection chips used here incorporate gold and reduced graphene oxide (rGO) coated surfaces. We demonstrate the system capability to monitor and record the biomolecular interaction between a typical protein bovine serum albumin (BSA) and these two substrates. This instrument was compared to a commercial QCM, demonstrating good correspondence between the computed mass adsorption density responses using the Sauerbrey model. For both Au and rGO surfaces, the custom QCM significantly outperforms the commercial system in limit of detection, sensitivity and linear range. The instrument presented here has the potential to serve as a ubiquitous bioelectronic tool for point-of-care disease screening and rapid therapeutics development.

* Corresponding author.
E-mail address: aravind@manchester.ac.uk (A. Vijayaraghavan).

https://doi.org/10.1016/j.aca.2021.338329
0003-2670/

1. Introduction

Standard biomedical instrumentation equipment and immunological research tools present limitations such as high cost, complexity of use and related steep learning curves that require highly skilled operators, and large size that makes point-of-care installation challenging, all of which hinders their use for early disease detection and delays medical interventions [1–3]. Their cost, complexity and use of proprietary technologies that limit field-serviceability also hinders their accessibility for low- and middle-income (LMI) countries. However, one route to develop easy-to-use, low-cost, adaptable and field-serviceable disease screening tools is to use affordable yet powerful embedded systems under open-source licensed ecosystems [3,4]. Modern embedded systems are not only capable of reading and converting the signals produced by different types of biosensors, but some platforms also offer internet connectivity that makes possible sharing data with practitioners in remote locations for real-time diagnosis under the Internet of Things (IoT) scheme of intelligent devices [5].

A biosensor is an analytical sensing device in which specific physiochemical changes that occur during the interaction between recognition bioelements such as proteins, enzymes or antibodies and an analyte are quantitatively converted into an electronic signal by a transducer [6,7]. Depending on the mechanism of transduction, a biosensor can be identified as optical, thermal, ion-sensitive, electrochemical or mass-sensitive, amongst others.

In this paper, we report on the development and evaluation of an inexpensive quartz crystal microbalance (QCM) instrument to study the biochemical binding interactions occurring at the sensor's surface. A QCM is a mass-sensitive technique based on the piezoelectric effect. It offers real-time and label-free capabilities for monitoring interfacial interactions with high sensitivity, quantifying mass adsorption events at the ng·cm^2 range [8–10]. Our instrument is based on the *openQCM* device (Novaetech, S.r.l, Italy), the first open-source QCM released under the Creative Commons license.

The QCM technique enables the modulation of the biomolecular adsorptions through the modification of the sensor's working electrode, which typically is made of a chromium-supported gold layer. Gold is a widely used material for biotechnological applications thanks to its inert chemical nature [11,12]. Invariably, gold substrates are coated with self-assembled monolayers (SAMs) to enable the biochemical functionalization by tailoring the hydrophilic or hydrophobic nature of the substrates [12–14]. For instance, SAMs of thiol chains can render the surface hydrophobic [15,16].

Graphene has recently attracted attention as a promising biosensor surface material due to its unique physical, chemical and electronic properties [17–21]. Graphene has been shown to improve the sensitivity of a biosensor thanks to its high specific surface area and electrical conductivity [21–24]. Reduced graphene oxide (rGO) is commonly obtained through chemical, photochemical or thermal deoxygenation of graphene oxide (GO) to obtain a material that resembles, to an extent, the properties of pristine graphene, including increased electrical conductivity and a highly hydrophobic surface. It has been shown that the performance of a biosensor can be tuned by modifying its surface with thin GO or rGO films where hydrophilic or hydrophobic interactions and π-π stacking are dominant forces at the interface [17,25–27]. We have previously reported on the formation of supported phospholipid monolayers and multilayers [28] as well the adsorption dynamics of bovine serum albumin (BSA) on rGO platforms [27] using the QCM with Dissipation monitoring (QCM-D) technique, where we revealed the pivotal role that the hydrophobicity and surface chemistries of the supporting substrates play during the adsorption events.

Despite the analytical advantages offered by monitoring the energy dissipation occurring at the QCM's interface during a mass adsorption event, the adsorption of small, rigid proteins may be effectively measured and quantified by exclusively monitoring frequency changes. For instance, serum albumins are small model proteins that are extensively used to prevent non-specific adsorption by blocking nonconjugated surfaces during a biosensing event [29]. Therefore, BSA was selected as the protein for the evaluation of the QCM instrument reported here.

We have developed an affordable custom QCM (cQCM) instrument based on the openQCM device. It is aimed at point-of-care operation for rapid detection and diagnosis based on protein-binding methodologies. Additionally, we equipped the cQCM with a custom-made electronic closed-loop control for temperature stabilization (Fig. 1). We assessed the stability of the instrument's response under controlled thermal conditions. Additionally, we evaluated our system through biomolecular adsorptions occurring at bare gold and graphene modified substrates. The sensors were conditioned and coated with GO and rGO films by following our procedure reported previously [28]. Finally, the results obtained with the cQCM were contrasted with a commercial QCM system with dissipation monitoring capabilities in order to validate the performance of our system. The resultant mass adsorption densities are comparable for both gold and graphene sensors, at a small fraction of the cost.

2. Materials and methods

2.1. Chemicals and materials

GO dispersion was prepared by a modified Hummers' method [30] followed by exfoliation and purification (see ESI 1). The stock dispersion of GO was diluted to a concentration of 0.8 mg/mL. Albumin, monomer bovine (A1900), and phosphate buffered solution (PBS) 0.1 M, pH 7.4 (P5244) (Sigma-Aldrich Canada) were used as received. Buffer solution was prepared dissolving 1 PBS tablet in 200 mL of ultrapure water. This solution was stirred for at least 30 min and filtered using sterile syringe filter units with a pore size of 0.22 μm (Millex-GP, PES membrane). This buffer solution was degassed using pulsated bath ultrasonication under vacuum for at least 1 h. BSA stock solution was prepared with a concentration of 5 mg/mL. Serial dilutions of BSA were prepared from the stock solution. A mild solution for initial cleaning of the QCM and QCM-D systems and quartz crystals was prepared with 2% SDS and Hellmanex II solution in MilliQ water. A stronger cleaning solution was prepared using the following reagents ratios: H_2O_2:NH_3:DI water = 1:1:5.

2.2. Equipment

2.2.1. QCM chips

All adsorptions measured using our cQCM instrument, driven by the openQCM device, were performed on Gold QCM sensors from Quartz Pro (Stockholm, Sweden) with a fundamental frequency of 10 MHz. For the QSense Pro (Biolin Scientific, Gothenburg, Sweden) system, QCM-D sensors with gold surface electrode (QSX-301, Biolin Scientific) and a fundamental frequency of 5 MHz were used. The value for the 3rd harmonic for both frequency ($\Delta f_{n=3}$) and energy dissipation ($\Delta D_{n=3}$) components were captured for comparative analysis.

To form GO thin films, a spin-coater (Laurell Tech., WS-650MZ) was used. Both QCM and QCM-D sensors were thoroughly cleaned according to the following procedure: QCM sensors were first soaked for at least 20 min in the 2% SDS/Hellmanex solution to

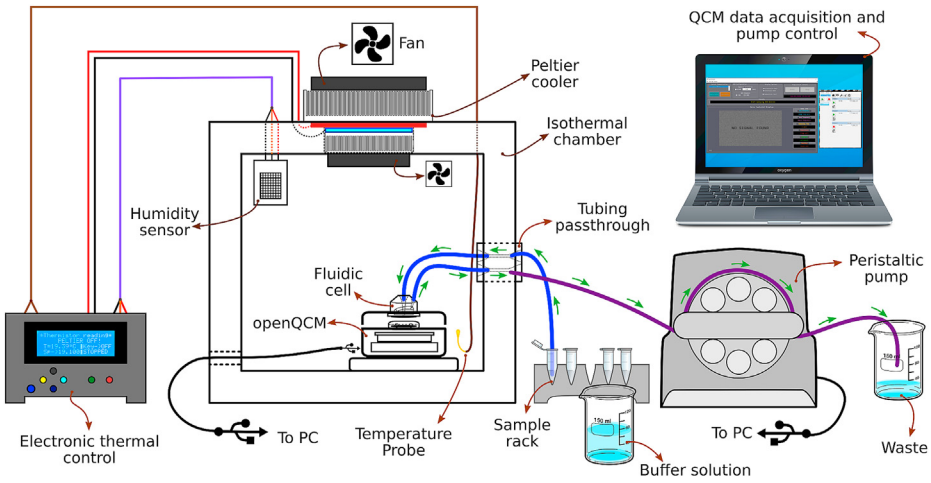

Fig. 1. Thermally stabilized cQCM laboratory instrument setup showing the openQCM device inside an isothermal chamber, Peltier cooler, temperature and humidity sensors and front panel of the custom-made electronic temperature control. A portable computer captures the QCM data through a custom GUI and controls the 3-channel peristaltic pump for sample flowing.

remove oil-based contaminants. This initial step is followed ultrasonication for 10 min in acetone, then isopropanol; intercalating DI water rinsing steps between each solution. Then, the crystals were treated under oxygen plasma at 80% power for 2 min (a 100W reference system is used). Using the strong cleaning solution, the crystals were soaked at 75 °C for 5 min. Finally, the sensors were rinsed with copious amounts of ultrapure water and dried with a mild stream of nitrogen gas before storing them in a dust-free and humidity-controlled environment before coating.

After the cleaning process, the crystals were coated with GO via spin coating (speed: 3000 rpm, acceleration: 350, 2 min) to form thin GO films on the chips. To obtain rGO-coated sensors, GO-precoated crystals were annealed at 180 °C under vacuum (~1 mBar) for 24 h (Townson+Mercer EV018 vacuum oven).

The degree of reduction was characterised via wetting contact angle (WCA) measurement (Kruss DSA100) of sessile drops (~5 μL) of DI water and X-ray photoelectron spectroscopy (XPS) using SPECS custom built system composed of a Phobios150 hemispherical electron analyser with 1D detector. The XPS data was analysed using CasaXPS software (version 2.3.18). The rGO sample for XPS was prepared using the same conditions used for the reduction of GO on QCM crystals. The GO was first casted and dried on the Si/SiO_2 (290 nm) substrate, followed by the reduction in vacuum at 180 °C for 20–25 h.

Scanning electron microscopy (SEM) was performed on a SEM Zeiss Ultra setup, using an acceleration voltage of 5 kV and a working distance of 5 mm. AFM topography images were acquired using a Bruker Alpha system in tapping mode with FastScan-A probes with a cantilever spring constant of 18 N/m.

2.2.2. cQCM system construction

The core monitoring device from our custom QCM instrument is the openQCM device. A detailed description of the principle of operation of this device is included in ESI 2.

A thermistor with a Negative Temperature Coefficient (NTC), (Vishay PN: NTCLE201E3103SB) with a room temperature resistance (R_0) of 10.00 kΩ and $\beta_{25/85}$ of 3977 was used as the temperature sensor for the isothermal chamber. It was configured in a voltage divider circuit (ESI Fig. S2) with a reference resistor with a value of 10.00 kΩ ±0.1%. A detailed description of the implemented instrumentation for temperature reading and digitization are included in ESI 3.1 and ESI 3.2, respectively. The humidity of the system was monitored during temperature stabilization. This humidity sensor (DHT22, Aosong Electronics) is an embedded digital device that uses a polymer capacitor as the sensing element and outputs the value of the sensor as a digital signal. A 20 W thermoelectric Peltier cooling assembly (AR-AR-019-12, Adaptive Thermal Management) was attached to a fully-insulated polystyrene (PS) box with the cold side facing inwards the box. A peristaltic pump (Ismatec Reglo ICC, 3 Ch) was placed after the QCM sensor to draw the liquid from the sample vials (Fig. 1) in order to minimise the formation of microbubbles.

A custom-made graphic user interface (GUI) was developed in Matlab R2018a to perform data acquisition, baseline calibration and data post-processing. ESI 4 describes the general functionalities and implementation of this software.

2.2.3. Development of a thermally stabilized QCM system

In order to accurately control the temperature of the inner atmosphere of the chamber, a Proportional Integral Derivative (PID) closed-loop control was implemented. Please refer to ESI 5 for a complete description of the PID control technique. The temperature control is driven by an Arduino Pro Micro microcontroller (ESI Fig. S3) board mounted on a custom-designed PCB. It captures and converts the readings from the thermistor, reads the user input for control parameters, processes the PID control algorithm and accordingly activates an electromechanical relay that powers the Peltier cooler. The temperature reported by the digital temperature sensor from the openQCM shield board showed an offset of 4.9 °C with respect to temperature registered by the NTC installed inside the chamber. This value was used as a correction factor in the firmware from the electronic control. ESI 6 provides a detailed description of the digital implementation of the temperature control algorithm.

2.2.4. Validation of the closed-loop thermal control

One of the few disadvantages of the openQCM device is that it presents an intrinsic self-heating effect that can be attributed to the simplicity of its construction. The processing unit, an Arduino Micro development board, which is in direct spatial contact with the printed circuit board that drives the QCM sensor, warms up after power-up affecting the frequency of oscillation over a defined stabilization period (<1 h). Therefore, the system was enclosed in an electronically-controlled thermal chamber in order to reduce

any thermal effects on the oscillations.

The first description of how capable the isothermal chamber is for keeping a stable temperature was done in terms of the frequency shift reported by the crystal during a low-to-high temperatures excursion on air. To do this, a clean crystal was mounted in the openQCM enclosure and a temperature of 13 °C was manually set on the controller and left overnight in order to ensure complete stability. Raw frequency values were captured and no liquid was flowed during this evaluation. Once the frequency and the temperature were stable, the QCM was let to warm up via its self-heating effect and the isothermal chamber was left to stabilize. When a frequency plateau was reached a new temperature was selected and the system left to stabilize again until a new stable frequency was reached. Five temperatures were configured during this evaluation: 13 °C, 15 °C, 20 °C, 24 °C and 30 °C.

A second analysis was performed during constant forced cooling to determine the thermal performance of the chamber. This evaluation would shed light on the change rate of the frequency with respect to the temperature until the QCM sensor reported a stable oscillating frequency once it reached a target temperature. From this result, a two-variable function, F(t,T) expresses the evolution of the resonant frequency in terms of the temperature decay during the period that the cQCM system usually takes to reach complete frequency stability (<2 h).

This examination was started by loading a clean Quartz Pro sensor in the cQCM enclosure, then the system was placed inside the isothermal chamber which had been left at room temperature. The board was powered on through the USB port of the acquisition computer and the crystal was left overnight to unperturbedly oscillate on air without thermal control so that the board could gradually self-heat. After ~12 h of stable oscillation, the board reported a maximum temperature of 34.1 °C. The acquisition was then restarted and after 10 min of capturing raw frequencies the thermal control was activated with a setpoint of 20 °C.

2.2.5. BSA protein adsorption study

Prior to every experiment a clean sensor was left inside the isothermal chamber for at least 1 h with the electronic control enabled in order to guarantee absolute stability. The overall resultant frequency dependence on the temperature was lower than 5 Hz/°C. Sample injection was kept at a continuous flow rate of 50 μL/min during 18 min, therefore approximately 850 μL were flowed over the crystal. Then, the buffer solution was flowed until the frequency reached good equilibrium (SD < 0.2). At the completion of the experimental routine, SDS 2% solution was flowed at 100 μL/min followed by ultrapure water at the same rate for at least 2 h to ensure complete cleanse of the fluidic circuit.

In order to provide contrasting evidence of the functionality of the system, the same concentrations and experimental conditions were used on the QSense Omega Pro system from Biolin Scientific using bare Au sensors.

3. Results and discussion

3.1. Characterisation of rGO-coated QCM sensors

SEM imaging reveals the topography of the GO film on the surface of the Au working electrode of QCM chips obtained by spin-coating. It is formed by a continuous film of overlapping flakes covering the entire surface (Fig. 2a), with film thicknesses varying from one to few monolayers. Fig. 2b shows sessile drops of DI water on the surface of the bare Au and rGO-coated QCM chips (Fig. 2c). The Au surface exhibits a hydrophilic property with a WCA of 41°±5° while the rGO surface is hydrophobic with a WCA of 85°±2°. XPS images for rGO coatings are presented in ESI 7. Refer to ESI 8 for AFM topography images from bare and coated sensors.

3.2. Thermal chamber evaluation

During this temperature dependence analysis, the onboard digital temperature sensor from the openQCM device showed a slight readout variation with respect to the selected values, as reported by the thermistor from the chamber, however the differences are mostly negligible as confirmed by their respective standard deviation (SD). Table 1 summarizes the results for the differences in temperature and the statistical evaluation of the results. Fig. 3 illustrates the results of this evaluation process. The sections highlighted with dotted squares on Fig. 3a are considered as regions of acceptable stability based on their flatness and the SD of the responses for both variables *f* and T. The observed overshoot in the frequencies may be attributable to a thermal inertial effect resulting from the specific thermal gradient of the whole system.

Fig. 3b includes two different fitting curves for the points obtained from the stability regions. The best-fitting curve is an exponential function that adjusts the obtained values for *F* and *T*. The linear fit was selected to represent the overall change rate of the frequency with respect to the total temperature change during the evaluation process. From this result it becomes evident that maintaining a constant temperature to reduce the observed self-heating effect throughout a whole experimental routine is crucial to preserve a flat frequency response. Moreover, this result justifies the necessity of thermally stabilizing the chamber before starting and during the whole duration of an experiment as well as maintaining a thermally unperturbed system.

The result for the continuous thermal evaluation over a period of 100 min is presented in Fig. 4. A manifest thermal drift is observed as a result of the temperature dependence of quartz resonators. The progress curves for frequency dependence on temperature change showed an initial rate period with linear trend (Fig. 4a), then both curves bend before reaching a stability region. The individual responses for frequency and temperature, $F(t)$ and $T(t)$ were then parametrized and plotted as$F(T)$ in Fig. 4b. This result demonstrates the impact of the temperature on the response of the QCM sensors. Interestingly, this trend is in line with the same evaluation presented in the seminal work from Sauerbrey [31] for the same type of QCM sensors used, AT-Cut crystal at 35° 15'' (please refer to Fig. 10 from Ref. [31]). When the temperature increases within the temperature range of 30 °C–40 °C, the frequency shows a semi-linear region with a negative change rate, equivalent to the trend discussed here.

The resultant slope shown in Fig. 4b, with an absolute value of 4.94 Hz/°C, can be refactored in terms of the resolution of our thermal control, equal to 0.0875 °C (see ESI 3.2). Therefore, the change rate of the frequency per Celsius is approximately 56.45 Hz/°C. Thus, the resultant temperature coefficient of frequency for our thermal control is 5.6 ppm/°C, for QCM sensors with a fundamental frequency of 10 MHz. This value represents the frequency stabilization capabilities of the designed isothermal chamber.

3.3. Protein adsorption studies with cQCM and QCM-D systems

3.3.1. QCM theory

In 1959, Sauerbrey demonstrated that upon adding mass to a QCM sensor surface a frequency decrease proportional to the added mass occurs and given that the mass is small compared to the total weight of the crystal the frequency change is directly proportional to the mass of the crystal (Eq. (1)) [31]. therefore their use as microbalances is based on the linear relationship between changes in the resonator mass and in the resonance frequency [31,32].

A detailed mathematical development of Eq. (1) is included in

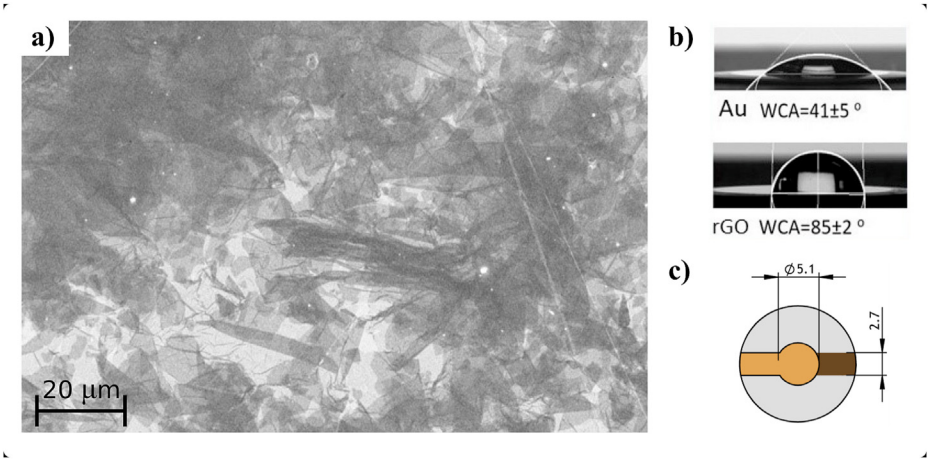

Fig. 2. a) SEM micrograph from rGO coated on Au QCM sensor. The working surface is fully covered with a varied number of graphene layers from one to few monolayers, b) Wetting contact angle (WCA) of bare Au and rGO-coated QCM sensors, c) Quartz Pro QCM sensors working electrode dimensions.

Table 1
Summary of mean temperature values and frequencies during the selected stabilization ranges.

Temperatures [°C]				Frequencies [Hz]	
Target Temp.	Obtained Mean Value	Difference	SD	Mean Value	SD
13	13.05	0.05	0.02	10,004,978.7	0.155
15	15.03	0.03	0.03	10,004,972.1	0.113
20	19.71	−0.29	0.07	10,004,963.1	0.176
24	24.67	0.67	0.02	10,004,956.7	0.137
30	29.17	−0.83	0.04	10,004,953.2	0.208

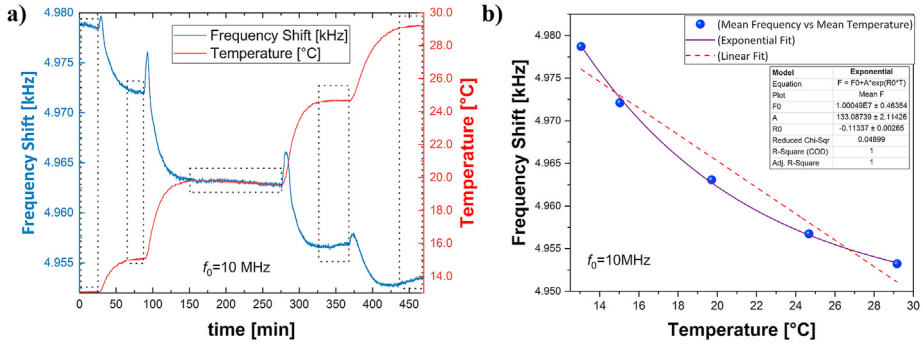

Fig. 3. Results for long thermal evaluation of the isothermal chamber. Vertical axis expressed the frequency shifts in kHz a) Thermal evaluation of the system's self-heating effect under controlled cooling. Temperature reported by the openQCM onboard sensor when controlling the temperature of the chamber upon self-heating, b) Temperature dependence of the frequency response of a QCM sensor under controlled cooling. Frequency vs Temperature response curve (●) for the data regions highlighted in (a) and two curve fits, linear and exponential, are shown and discussed in the text. Crystal's fundamental frequency, f_0 = 10 MHz.

ESI 9.

Several reports have demonstrated the possibility to study the adsorptions of small proteins using conventional QCM surfaces due to the rigid coupling of some proteins to the substrate obtaining negligible or low viscoelastic characteristics, therefore allowing the use of the Sauerbrey model [33–35]. However, it is important to acknowledge that no absolute standard exist to establish dissipation as negligible. An often-used rule of thumb is that the Sauerbrey equation gives a correct value for mass added if the associated dissipation value with the adlayer is less than 2×10^{-6} [36,37]. The dissipation values reported in the literature for the adsorption of BSA onto QCM-D substrates meet this criterion [38–40].

3.3.2. Protein adsorption on Au and rGO

Once the cQCM instrument was thermally stable, it was used to measure the adsorption of different BSA protein concentrations, ranging from 10 μg/mL to 1000 μg/mL on QCM surfaces. Two substrates with different surface chemistries, Au and rGO were used for these adsorption studies. The humidity of the chamber throughout these experiments was registered in the project workbook with an average value below 65%. The overall temperature for the QCM experiments described here was 20.3 $°C$ ±0.0014$°C$. Fig. 5a–b presents the results from the adsorptions of BSA on bare Au and rGO-coated QCM sensors, respectively. Similarly, Fig. 5c–d presents the same pair for the QSense system.

On bare Au, during BSA adsorption the frequency increasingly

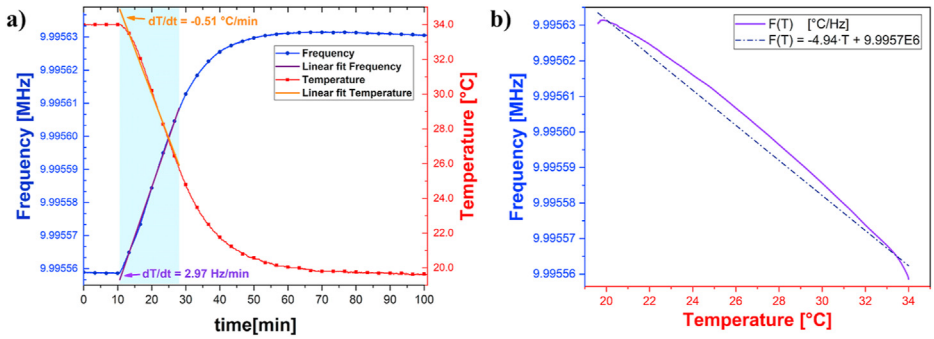

Fig. 4. Results for the continuous cooling of the openQCM system a) QCM frequency response at continuous temperature decrease. Frequency response and temperature evolution over time. Both frequency and temperature present a linear region (in light blue) with change rates of 2.97 Hz/min and −0.51 °C/min, respectively, b) Frequency vs temperature (F(T)) characteristic. (For interpretation of the references to colour in this figure legend, the reader is referred to the Web version of this article.)

$$\frac{\Delta m}{A} = -\frac{\sqrt{\rho_Q \mu_Q}}{2f_0^2}\Delta f \quad [g/cm^2] \tag{1}$$

shifts with respect to the degree of protein concentration. Fig. 5a shows the QCM measurements for BSA adsorption on Au using our cQCM instrument. The total frequency shifts for all concentration of BSA are from about 10 Hz to 500 Hz. Similarly, the results from the QSense system show an increase on the frequency shift and adsorption rate as the concentration of protein is increased, (Fig. 5c). However, the range of the total frequency shifts for all concentrations lies between 4 and 35 Hz, which are considerably lower than those obtained with our cQCM.

Fig. 5b corresponds to the adsorption of BSA onto a rGO-coated sensor using our cQCM. For a BSA concentration of 10 μg/mL, the curve shows a fast adsorption rate at the initial stage followed by a notably slow adsorption, as the change of frequency is almost flat. The total frequency shift after the rinsing process is approximately 20 Hz. For BSA concentrations of 20 μg/mL and 50 μg/mL, a fast adsorption rate at the initial stage is followed by no further adsorption after a few minutes, as evidenced by the flat frequency shift. The total frequency shift in both cases are similar at approximately 32 Hz. With a BSA concentration of 100 μg/mL, the adsorption rate is initially high then slows down after a few minutes, resulting in a total frequency shift of about 40 Hz. For the highest used BSA concentration of 1000 μg/mL, the protein was rapidly adsorbed onto the surface with a frequency shift of approximately 140 Hz, then no more adsorption was observed, as noted by the flat frequency response.

Similar to the results obtained with our cQCM system, the

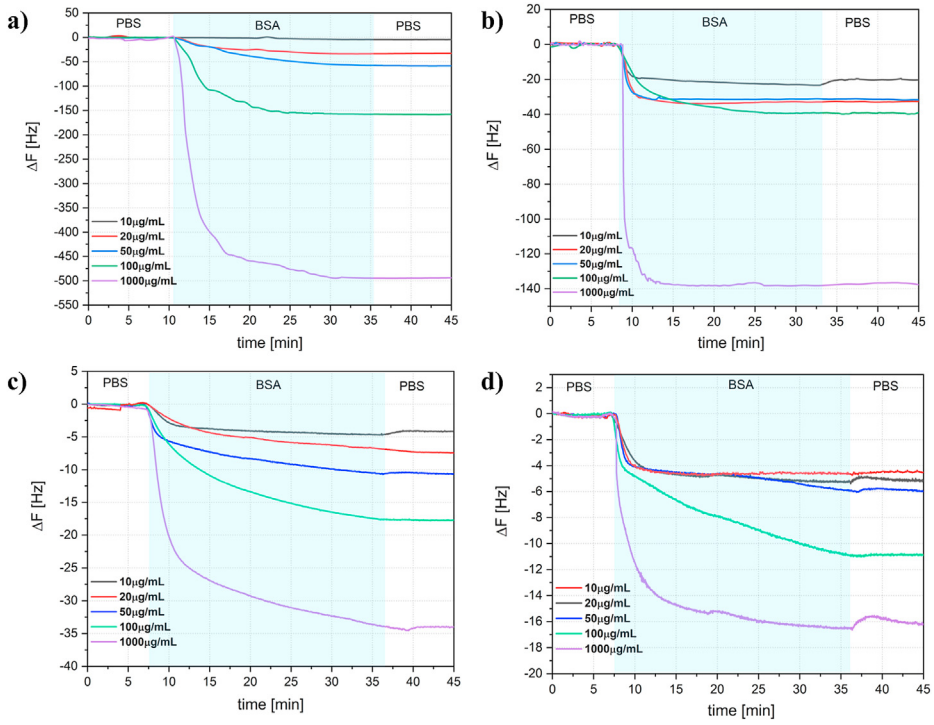

Fig. 5. QCM results for the adsorptions of BSA on a) bare Au and b) rGO-coated using the cQCM, c) and d) present the same pair for the QSense system.

adsorption of BSA on rGO-coated sensors measured with the QSense system shows different adsorption characteristics depending on the concentration of the protein. For low concentrations of BSA (10, 20, 50 μg/mL), the adsorption shows a comparable trend: fast adsorption rate at the initial stage followed by a slower adsorption after a few minutes, as the frequency responses are almost flat. The total frequency shifts for those three cases are about 5 Hz. In contrast, for a BSA concentration of 100 μg/mL, the graphs shows a 2-stage adsorption with different adsorption rates. The initial stage presents a fast adsorption rate with an intermediate frequency shift of about 5 Hz, then the adsorption rate decreases and the frequency changes homogenously reaching a plateau at 11 Hz. For a BSA concentration of 1000 μg/mL, the protein was rapidly adsorbed onto the surface, then slowed down reaching a total frequency shift of approximately 17 Hz.

The adsorption kinetics obtained from both systems are fairly similar, observing a 2-stage adsorption for 100 μg/mL BSA onto rGO. We have recently evidenced this behaviour in a systematic study of the adsorption of BSA on graphene platforms [27]. At this point is important to highlight the differences on the sample injection/flowing methods as they can render specific hydrodynamic pressure profiles. While our system uses a peristaltic pump that withdraws liquid from the sample vials (Fig. 1), the QSense system uses top-injection and lateral-withdrawal syringe pumps with precision motorized stages.

3.3.3. Mass adsorption and comparison with QSense

A comparative evaluation of the adsorption of BSA with the same five concentrations using the QSense system is presented. The total aerial mass density adsorption was obtained from the Sauerbrey equation (Eq. (1)) for both frequency responses and are shown in Fig. 6. Quantitatively, the mass densities obtained using both systems show similar trends and their magnitudes are comparable within the margins of error for both gold and rGO surfaces. For the adsorption on rGO surface, the adsorption mass of all concentrations, calculated from QSense results, are slightly higher than those measured from our in-house system probably due to the topographical differences between the two types of crystals, QSense vs. Quartz Pro.

3.3.4. Discussion

BSA can be modelled as an oblate ellipsoid with approximate dimensions 4 nm × 4 nm × 14 nm in aqueous solution with molecular weight of 66 kDa [41]. BSA adsorbs with specific orientations leading to specific adsorption kinetics when in contact with substrates with different chemistries [42]. On this regard, we have recently demonstrated the effects of gradual reduction degrees of rGO and the effects of protein concentrations on the adsorption kinetics on graphene derivatives [27]. The adsorption of BSA molecules onto a surface can occur in two orthogonal extreme orientations: side-on and end-on. If a side-on orientation is considered, one BSA molecule will occupy an approximate area of 56 nm^2, resultant from a projection on the X–Y plane of the prism that circumscribes the model ellipsoidal shape of the protein, obtaining then a rectangle [40,41]. This results in a maximal density of 1.78×10^{12} BSA molecules per cm^2 or 194 ng/cm^2 for the monolayer side-on arrangement. For the end-on scenario, a BSA molecule occupies an approximate area of 16 nm^2 corresponding to 9.63×10^{12} BSA molecules per cm^2 or 685 ng/cm^2 for the monolayer end-on adsorption.

On a gold sensing surface, the mass adsorption for the BSA concentration 10 μg/mL to 1000 μg/mL ranges from 40 ng/cm^2 to 800 ng/cm^2. For the case of BSA concentrations lower than 100 μg/mL, a side-on deposition with denaturation on gold of the protein can be assumed. On this regard, McArdle et al. [43] studied the effect of concentration of MvBOx to bare and SAM-modified surfaces using QCM and DPI, claiming that at lower concentrations the protein has time to relax on the surface and form a more rigid layer due to the lack of electrostatic repulsion from the presence of neighbouring proteins and extensive denaturation of the protein occurs in the case of low concentrations (100 μg/mL).

For BSA at a high concentration environment, the observed high amounts of adsorbed mass could be due to water entrapment into the protein layers [40,44]. The interaction between BSA and gold could originate from disulphide bonds and hydrophobic interaction. As BSA contain 17 disulphide bonds in the molecule, it is likely to bind with Au via at least one thiol originating the disulphide bonds [45]. Several reports on the interaction of BSA with Au have stressed out the importance of the maximization of hydrophobic interactions as a crucial factor in the irreversible adsorption of proteins [38,41].

In contrast, on rGO surfaces, the mass adsorption ranges from 30 ng/cm^2 to 300 ng/cm^2 for the concentration range used in this study. The adsorption mass on rGO surface is relatively lower than that on gold surface. It is assumed that deposited BSA molecules flattened and denatured on rGO surfaces due to the strong

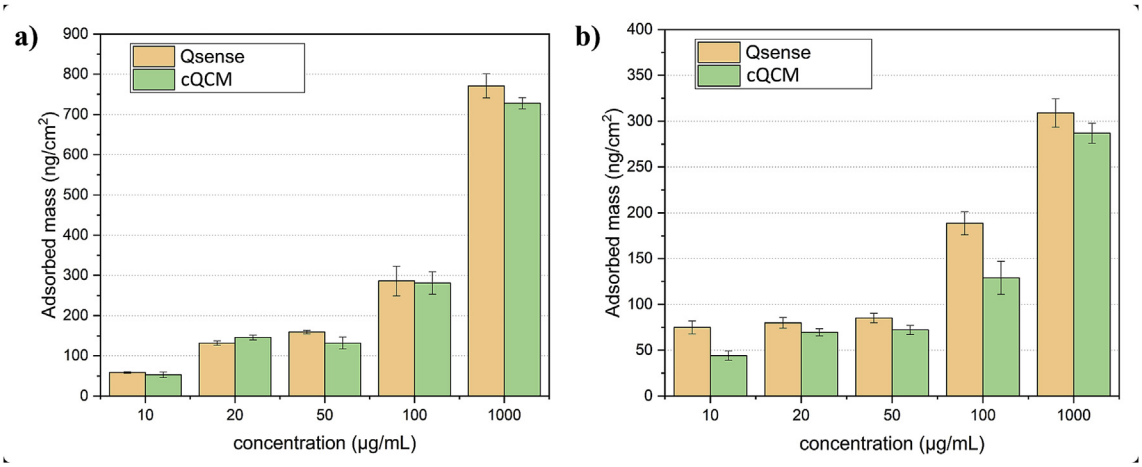

Fig. 6. BSA mass adsorption densities comparison on a) bare Au and b) rGO-coated sensors. Results for the cQCM instrument are shown in green bars while QSense results correspond to the orange bars. See online version for colour. (For interpretation of the references to colour in this figure legend, the reader is referred to the Web version of this article.)

hydrophobic interaction with rGO resulting in lower adsorbed mass [27]. A two-stage adsorption process in the case of BSA concentration higher than 100 μg/mL could have begun with the formation of a rigid layer, where the spreading of molecules is higher, followed then by the formation of an additional layer of BSA molecules [27,43]. Interestingly, an initial fast adsorption rate of low BSA concentrations (<50 μg/mL) on rGO surfaces is observed. It is believed that this effect is due to predominant hydrophobic interactions between rGO and the hydrophobic functional groups of BSA in addition to π-π stacking processes, which in turn flatten the protein molecules, saturating the surface of the working electrode [27,46,47].

Table 2 summarizes the evaluation of the performance of our system, including the limit of detection, sensitivity and linear ranges for the concentrations studied, for both surfaces. The complete set of calibration curves used to obtain these values is included in ESI 10.

The limit of detection (LOD) was computed using the 3-sigma method, according to Eq. (2).

$$LOD = \frac{3\sigma}{S_{LR}} \quad [\mu g / mL] \tag{2}$$

where σ is the standard deviation (SD) of the response from blank sensors and S_{LR} is the slope from the Linear Range (LR) of the respective calibration curves.

In general, the cQCM system offers higher sensitivity, lower detection limits and wider linear range compared to the QSense system.

The highest sensitivity was observed on the bare Au substrate with the cQCM system. The resultant ΔF vs concentration pairs for both cQCM and QSense systems were plotted and fitted using Hill curve fitting, a widely used model to describe occupancy of biomolecules on surfaces, like BSA-Au [48]. The linear regions from bare Au substrates lie within the concentration range of 10 μg/mL to 100 μg/mL, obtained from the fitted sigmoidal curves for both systems.

Interestingly, rGO-coated substrates present a relatively wider range of linearity compared to bare-Au. It is reasoned that a thin film of squashed BSA molecules forms on the rGO surface followed by the stacking of an additional layer of BSA, exposing more hydrophilic regions where more molecules can be adsorbed [27]. This results in the increase of the molecular saturation point of the crystal. On bare-Au, in contrast, the crystal reaches a faster BSA saturation without molecular flattening as the concentration increases, matching the Hill model.

In terms of the LOD, values of ~6.8 μg/mL and ~9.8 μg/mL were obtained for the cQCM and QSense systems, respectively. The rGO surface in the cQCM system linearly responded within the concentration range of 20 μg/mL to 1000 μg/mL while the QSense system reported a lower linear range from 50 μg/mL to 1000 μg/mL, for the rGO surface. This difference is attributed to the intrinsic properties of the QSense and cQCM systems i.e. hydrodynamic pressure, noise floor, sensor fundamental frequency and sensor instrumentation principle.

4. Conclusions

We have evaluated the performance of a thermally stabilized open source-based QCM instrument through protein adsorptions. The designed instrument is targeted at biomolecular interactions studies with field-operability capacity at an affordable total cost of ~£2000. It was observed that a continuous cooling process has a stronger effect on the frequency stabilization rate compared to that for forced cooling upon self-heating. In the linear fittings for the two responses of $F(T)$ (Figs. 3b and 4b), the discrete evaluation showed a slope of −1.5477 ± 0.1988 Hz/°C while the continuous cooling showed a change ratio of −4.94 ± 0.01082 Hz/°C, which represents an increase in the cooling capability by a factor of ~3. The overall humidity of the chamber throughout these experiments was below 65%. In spite of the low SD for the temperatures obtained for the BSA adsorption studies and the good temperature stability during the lifetime of each experimental session, there is a possibility of increasing the accuracy of the target temperature by interfacing the readout value from the openQCM board to the PID control via the GUI for data acquisition. In this way, the chamber sensor would be bypassed as the QCM temperature monitoring device and the control could be driven by the temperature reported by the openQCM's on-board digital sensor. This new approach would eliminate the resultant offset from the temperatures reported by the two sensors and, in consequence, the efficacy of the thermal control would significantly improve. Additionally, it is possible to increase the granularity of the temperature reading by changing to an external 12-bit or higher resolution ADC module.

In spite of the fact that the cQCM system presented here inherently lacks dissipation monitoring capabilities, it showed higher sensitivity and lower detection limits compared to the commercial system and at a much lower cost. It was observed that the adsorption dynamics strongly depends on the protein concentrations and surface chemistries. Particularly, rGO-coated QCM sensors present relatively wider range of linearity for BSA adsorption compared to bare-Au as an additional protein layer is formed promoting hydrophilic regions where more molecules can be adsorbed. This can be useful to tailor QCM-based biomolecular assays, as we have recently demonstrated on the development of a Point-of-Care immunosensor for membranous nephropathy [49].

The functionalization of QCM substrates with biochemical species, including the formation of rGO-supported biotinylated lipid monolayers [28] or the use of "reporter" molecules can be explored. This integrated system presents an opportunity for materials scientists, biomedical engineers or practitioners for studying chemical and biomolecular interactions with surfaces. Moreover, it can help to develop label-free, fast and low-cost immunoassays readily available for homecare use without requiring extensive training. It has the potential to become a fast and highly sensitive point-of-care diagnostic instrument especially well-suited for low- and middle-income countries. Future upgrades will endow the instrument with multi-channel reading of bio-functionalised sensors, reversible chamber cooling and heating, machine learning for data processing, and mobile access with both cloud- and host-based computing capabilities.

Table 2
Summary of sensitivity, limits of detection and linear ranges for the cQCM and QSense systems.

System	Surface	LOD (μg/mL)	Sensitivity (Hz/μgmL^{-1})	Linear Range (μg/mL)
cQCM	Bare Au	~2.6	1.63	10–100
	rGO	~6.8	0.10	20–1000
QSense	Bare Au	~4.4	0.14	10–100
	rGO	~9.8	0.01	50–1000

Credit authorship contribution statement

Daniel Melendrez: conceptualization, investigation, software, validation, data curation, formal analysis, writing - original draft, writing – review & editing, funding acquisition. Piramon Hampitak: investigation, methodology, data curation, formal analysis, writing – original draft, writing – review & editing, funding acquisition. Thomas Jowitt: supervision, methodology, resources. Maria Iliut: investigation, resources, writing – review & editing. Aravind Vijayaraghavan: conceptualization, methodology, supervision, writing - original draft, writing – review & editing, project administration, funding acquisition.

CRediT authorship contribution statement

Daniel Meléndrez: Conceptualization, Methodology, Software, Validation, Formal analysis, Investigation, Writing – original draft, Writing – review & editing, Visualization. **Piramon Hampitak:** Conceptualization, Methodology, Validation, Formal analysis, Investigation, Writing – original draft, Writing – review & editing. **Thomas Jowitt:** Conceptualization, Methodology, Validation, Data curation, Resources, Writing – original draft, Writing – review & editing, Supervision, Project administration, Funding acquisition. **Maria Iliut:** Investigation, Writing – original draft, Writing – review & editing. **Aravind Vijayaraghavan:** Conceptualization, Methodology, Validation, Data curation, Resources, Writing – original draft, Writing – review & editing, Supervision, Project administration, Funding acquisition.

Declaration of competing interest

The authors declare that they have no known competing financial interests or personal relationships that could have appeared to influence the work reported in this paper.

Acknowledgments

D.M. acknowledges The National Council for Science and Technology (CONACyT), Mexico for the financial support. D.M. thanks Marco Mauro from Novaetech (openQCM team) for the technical support and feedback provided during the course of this research. P.H. acknowledges the financial support of the Development and Promotion of Science and Technology Talents Project (DPST), Thailand. We acknowledge the support of the Biomolecular Analysis Core Facility, Faculty of Biology Medicine and Health, The University of Manchester. A.V. acknowledges funding from the Engineering & Physical Sciences Research Council (EP/K016946/1).

Appendix A. Supplementary data

Supplementary data to this article can be found online at https://doi.org/10.1016/j.aca.2021.338329.

References

[1] D. Battal, S. Akgönüllü, M.S. Yalcin, H. Yavuz, A. Denizli, Molecularly imprinted polymer based quartz crystal microbalance sensor system for sensitive and label-free detection of synthetic cannabinoids in urine, Biosens. Bioelectron. 111 (2018) 10–17, https://doi.org/10.1016/j.bios.2018.03.055.
[2] A. Fatoni, A.N. Aziz, M.D. Anggraeni, Low-cost and real-time color detector developments for glucose biosensor, Sens. Bio-Sensing Res. 28 (2020), 100325, https://doi.org/10.1016/j.sbsr.2020.100325.
[3] Y.D. Han, H.J. Chun, H.C. Yoon, Low-cost point-of-care biosensors using common electronic components as transducers, Biochip J 14 (2020) 32–47, https://doi.org/10.1007/s13206-020-4104-8.
[4] W. Senbua, J. Mearnchu, J. Wichitwechkarn, Easy-to-use and reliable absorbance-based MPH-GST biosensor for the detection of methyl parathion pesticide, Biotechnol. Reports 27 (2020), e00495, https://doi.org/10.1016/j.btre.2020.e00495.
[5] V. Puri, R. Kumar, D. Nhuong Le, S.S. Jagdev, N. Sachdeva, BioSenHealth 2.0–a Low-Cost, Energy-Efficient Internet of Things–Based Blood Glucose Monitoring System. Emergence of Pharmaceutical Industry Growth with Industrial IoT Approach, Elsevier Inc, 2020.
[6] S.P. Mohanty, Biosensors : a tutorial review Biosensors : a tutorial review, IEEE Potentials 25 (2015) 35–40, https://doi.org/10.1109/MP.2006.1649009.
[7] J.M. Moon, N. Thapliyal, K.K. Hussain, R.N. Goyal, Y.B. Shim, Conducting polymer-based electrochemical biosensors for neurotransmitters: a review, Biosens. Bioelectron. 102 (2018) 540–552, https://doi.org/10.1016/j.bios.2017.11.069.
[8] M. Rodahl, F. Höök, A. Krozer, P. Brzezinski, B. Kasemo, Quartz crystal microbalance setup for frequency and Q-factor measurements in gaseous and liquid environments, Rev. Sci. Instrum. 66 (1995) 3924–3930, https://doi.org/10.1063/1.1145396.
[9] J.W. Thies, P. Kuhn, B. Thürmann, S. Dübel, A. Dietzel, Microfluidic quartz-crystal-microbalance (QCM) sensors with specialized immunoassays for extended measurement range and improved reusability, Microelectron. Eng. 179 (2017) 25–30, https://doi.org/10.1016/j.mee.2017.04.023.
[10] Z. Zhang, Q. Dou, S. Wang, D. Hu, X. Guo, B. Liao, Z. Zhao, H. Liu, Q. Dai, Hybrid hydrogel films with graphene oxide for continuous saliva-level monitoring, J. Mater. Chem. C 8 (2020) 9655–9662, https://doi.org/10.1039/d0tc00725k.
[11] P.M. Wolny, J.P. Spatz, R.P. Richter, B. Unit, P. Miramon, D. Sebastian, On the adsorption behavior of biotin-binding, Proteins on Gold and Silica 26 (2010) 1029–1034, https://doi.org/10.1021/la902226b.
[12] J.T. Marquês, R.F.M. De Almeida, A.S. Viana, Lipid bilayers supported on bare and modified gold - formation, characterization and relevance of lipid rafts, Electrochim. Acta 126 (2014) 139–150, https://doi.org/10.1016/j.electacta.2013.07.117.
[13] L. Newton, T. Slater, N. Clark, A. Vijayaraghavan, Self assembled monolayers (SAMs) on metallic surfaces (gold and graphene) for electronic applications, J. Mater. Chem. C 1 (2013) 376–393, https://doi.org/10.1039/C2TC00146B.
[14] M. Pohanka, QCM immunosensor for the determination of Staphylococcus aureus antigen, Chem. Pap. 74 (2020) 451–458, https://doi.org/10.1007/s11696-019-00889-5.
[15] C.A. Keller, B. Kasemo, Surface specific kinetics of lipid vesicle adsorption measured with a quartz crystal microbalance, Biophys. J. 75 (1998) 1397–1402, https://doi.org/10.1016/S0006-3495(98)74057-3.
[16] R. Hajiraissi, M. Hanke, Y. Yang, B. Duderija, A. Gonzalez Orive, G. Grundmeier, A. Keller, Adsorption and fibrillization of islet amyloid polypeptide at self-assembled monolayers studied by QCM-D, AFM, and PM-IRRAS, Langmuir 34 (2018) 3517–3524, https://doi.org/10.1021/acs.langmuir.7b03626.
[17] C.I.L. Justino, A.R. Gomes, A.C. Freitas, A.C. Duarte, T.A.P. Rocha-Santos, Graphene based sensors and biosensors, TrAC Trends Anal. Chem. (Reference Ed.) 91 (2017) 53–66, https://doi.org/10.1016/j.trac.2017.04.003.
[18] M.B. Lerner, D. Pan, Y. Gao, L.E. Locascio, K.Y. Lee, J. Nokes, S. Afsahi, J.D. Lerner, A. Walker, P.G. Collins, K. Oegema, F. Barron, B.R. Goldsmith, Large scale commercial fabrication of high quality graphene-based assays for biomolecule detection, Sensor. Actuator. B Chem. 239 (2017) 1261–1267, https://doi.org/10.1016/j.snb.2016.09.137.
[19] S. Afsahi, M.B. Lerner, J.M. Goldstein, J. Lee, X. Tang, D.A. Bagarozzi, D. Pan, L. Locascio, A. Walker, F. Barron, B.R. Goldsmith, Novel graphene-based biosensor for early detection of Zika virus infection, Biosens. Bioelectron. 100 (2018) 85–88, https://doi.org/10.1016/j.bios.2017.08.051.
[20] D. Susilo, T. Mujiono, Darminto, QCM coating with rGO material as a platform developing piezoelectric biosensor, in: Proc. - 2019 Int. Semin. Intell. Technol. Its Appl, ISITIA, 2019, https://doi.org/10.1109/ISITIA.2019.8937178, 2019 52–55.
[21] L. Xu, Y. Wen, S. Pandit, V.R.S.S. Mokkapati, I. Mijakovic, Y. Li, M. Ding, S. Ren, W. Li, G. Liu, Graphene-based biosensors for the detection of prostate cancer protein biomarkers: a review, BMC Chem 13 (2019) 1–12, https://doi.org/10.1186/s13065-019-0611-x.
[22] C. Chung, Y.K. Kim, D. Shin, S.R. Ryoo, B.H. Hong, D.H. Min, Biomedical applications of graphene and graphene oxide, Acc. Chem. Res. 46 (2013) 2211–2224, https://doi.org/10.1021/ar300159f.
[23] M.H. Mat Zaid, J. Abdullah, N.A. Yusof, Y. Sulaiman, H. Wasoh, M.F. Md Noh, R. Issa, PNA biosensor based on reduced graphene oxide/water soluble quantum dots for the detection of Mycobacterium tuberculosis, Sensor. Actuator. B Chem. 241 (2017) 1024–1034, https://doi.org/10.1016/j.snb.2016.10.045.
[24] D.P. Singh, C.E. Herrera, B. Singh, S. Singh, R.K. Singh, R. Kumar, Graphene oxide: an efficient material and recent approach for biotechnological and biomedical applications, Mater. Sci. Eng. C 86 (2018) 173–197, https://doi.org/10.1016/j.msec.2018.01.004.
[25] J.N. Dash, R. Jha, On the performance of graphene-based D-shaped photonic crystal fibre biosensor using surface plasmon resonance, Plasmonics 10 (2015) 1123–1131, https://doi.org/10.1007/s11468-015-9912-7.
[26] V. Georgakilas, J.N. Tiwari, K.C. Kemp, J.A. Perman, A.B. Bourlinos, K.S. Kim, R. Zboril, Noncovalent functionalization of graphene and graphene oxide for energy materials, biosensing, catalytic, and biomedical applications, Chem. Rev. 116 (2016) 5464–5519, https://doi.org/10.1021/acs.chemrev.5b00620.
[27] P. Hampitak, D. Melendrez, M. Iliut, M. Fresquet, N. Parsons, B. Spencer, T.A. Jowitt, A. Vijayaraghavan, Protein interactions and conformations on graphene-based materials mapped using quartz-crystal microbalance with dissipation monitoring (QCM-D), Carbon N. Y. 165 (2020b) 317–327, https://

doi.org/10.1016/j.carbon.2020.04.093.
[28] D.A. Melendrez, T. Jowitt, M. Iliut, A.F. Verre, S. Goodwin, A. Vijayaraghavan, Adsorption and binding dynamics of graphene-supported phospholipid membranes using the QCM-D technique, Nanoscale 10 (2018) 2555–2567, https://doi.org/10.1039/C7NR05639G.
[29] X. Deng, M. Chen, Q. Fu, N.M.B. Smeets, F. Xu, Z. Zhang, C.D.M. Filipe, T. Hoare, A highly sensitive immunosorbent assay based on biotinylated graphene oxide and the quartz crystal microbalance, ACS Appl. Mater. Interfaces 8 (2016) 1893–1902, https://doi.org/10.1021/acsami.5b10026.
[30] W.S. Hummers, R.E. Offeman, Preparation of graphitic oxide, J. Am. Chem. Soc. 80 (1958), https://doi.org/10.1021/ja01539a017, 1339–1339.
[31] G. Sauerbrey, Verwendung von Schwingquarzen zur Wägung dünner Schichten und zur Mikrowägung, Zeitschriftfür Phys. 155 (1959) 206–222, https://doi.org/10.1007/BF01337937.
[32] M. Edvardsson, M. Rodahl, B. Kasemo, F. Ho, A dual-frequency QCM-D Setup Operating at Elevated Oscillation Amplitudes, Analytical chemistry 77 (2005) 4918–4926, https://doi.org/10.1021/ac050116j.
[33] M.C. Dixon, Quartz crystal microbalance with dissipation monitoring: enabling real-time characterization of biological materials and their interactions, J. Biomol. Tech. 19 (2008) 151–158.
[34] N. Chandrasekaran, S. Dimartino, C.J. Fee, Study of the adsorption of proteins on stainless steel surfaces using QCM-D, Chem. Eng. Res. Des. 91 (2013) 1674–1683, https://doi.org/10.1016/j.cherd.2013.07.017.
[35] B. Salih, M.Y. Arica, U. Guler, V.C. Ozalp, G. Bayramoglu, M. Yilmaz, Lysozyme specific aptamer immobilized MCM-41 silicate for single-step purification and quartz crystal microbalance (QCM)-based determination of lysozyme from chicken egg white, Microporous Mesoporous Mater. 207 (2015) 95–104, https://doi.org/10.1016/j.micromeso.2015.01.009.
[36] X. Sha, C. Sun, X. Xu, L. Alexander, P.J. Loll, L.S. Penn, Quartz crystal microbalance (QCM): useful for developing procedures for immobilization of proteins on solid surfaces, Anal. Chem. 84 (2012) 10298–10305, https://doi.org/10.1021/ac302275r.
[37] X. Huang, Q. Bai, J. Hu, D. Hou, A practical model of quartz crystal microbalance in actual applications, Sensors 17 (2017) 1–9, https://doi.org/10.3390/s17081785.
[38] A.A. Feiler, A. Sahlholm, T. Sandberg, K.D. Caldwell, Adsorption and viscoelastic properties of fractionated mucin (BSM) and bovine serum albumin (BSA) studied with quartz crystal microbalance (QCM-D), J. Colloid Interface Sci. 315 (2007) 475–481, https://doi.org/10.1016/j.jcis.2007.07.029.
[39] B. Beykal, M. Herzberg, Y. Oren, M.S. Mauter, Influence of surface charge on the rate, extent, and structure of adsorbed Bovine Serum Albumin to gold electrodes, J. Colloid Interface Sci. 460 (2015) 321–328, https://doi.org/10.1016/j.jcis.2015.08.055.
[40] B. Jachimska, K. Tokarczyk, M. Łapczyńska, A. Puciul-Malinowska, S. Zapotoczny, Structure of bovine serum albumin adsorbed on silica investigated by quartz crystal microbalance, Colloids Surf. A Physicochem. Eng. Asp. 489 (2016) 163–172, https://doi.org/10.1016/j.colsurfa.2015.10.033.
[41] H.T.M. Phan, S. Bartelt-Hunt, K.B. Rodenhausen, M. Schubert, J.C. Bartz, Investigation of bovine serum albumin (BSA) attachment onto self-assembled monolayers (SAMs) using combinatorial quartz crystal microbalance with dissipation (QCM-D) and spectroscopic ellipsometry (SE), PloS One 10 (10) (2015), e0141282, https://doi.org/10.1371/journal.pone.0141282.
[42] M. Tencer, R. Charbonneau, N. Lahoud, P. Berini, AFM study of BSA adlayers on Au stripes, Appl. Surf. Sci. 253 (2007) 9209–9214, https://doi.org/10.1016/j.apsusc.2007.05.079.
[43] T. McArdle, T.P. McNamara, F. Fei, K. Singh, C.F. Blanford, Optimizing the mass-specific activity of bilirubin oxidase adlayers through combined electrochemical quartz crystal microbalance and dual polarization interferometry analyses, ACS Appl. Mater. Interfaces 7 (2015) 25270–25280, https://doi.org/10.1021/acsami.5b07290.
[44] M.M. Ouberai, K. Xu, M.E. Welland, Effect of the interplay between protein and surface on the properties of adsorbed protein layers, Biomaterials 35 (2014) 6157–6163, https://doi.org/10.1016/j.biomaterials.2014.04.012.
[45] S.B. Thourson, C.A. Marsh, B.J. Doyle, S.J. Timpe, Quartz crystal microbalance study of bovine serum albumin adsorption onto self-assembled monolayer-functionalized gold with subsequent ligand binding, Colloids Surf. B Biointerfaces 111 (2013) 707–712, https://doi.org/10.1016/j.colsurfb.2013.06.053.
[46] J. Guo, X. Yao, L. Ning, Q. Wang, H. Liu, The adsorption mechanism and induced conformational changes of three typical proteins with different secondary structural features on graphene, RSC Adv. 4 (2014) 9953–9962, https://doi.org/10.1039/c3ra45876h.
[47] S. Wang, X. Ou, Y. Wutthinitikornkit, M. Yi, J. Li, Effects of the surface polarity of nanomaterials on their interaction with complement protein gC1q, RSC Adv. 10 (2020) 41993–42000, https://doi.org/10.1039/d0ra05493c.
[48] A.M. Davidson, M. Brust, D.L. Cooper, M. Volk, Sensitive analysis of protein adsorption to colloidal gold by differential centrifugal sedimentation, Anal. Chem. 89 (2017) 6807–6814, https://doi.org/10.1021/acs.analchem.7b01229.
[49] P. Hampitak, T.A. Jowitt, D. Melendrez, M. Fresquet, P. Hamilton, M. Iliut, K. Nie, B. Spencer, R. Lennon, A. Vijayaraghavan, A point-of-care immunosensor based on a quartz crystal microbalance with graphene biointerface for antibody assay, ACS Sens. 5 (2020a) 3520–3532, https://doi.org/10.1021/acssensors.0c01641.